MOLECULAR AND CELLULAR BIOLOGY, Jan. 2003, p. 462–473 Vol. 23, No. 2
0270-7306/03/$08.00+0 DOI: 10.1128/MCB.23.2.462–473.2003

mdm2 Is Critical for Inhibition of p53 during Lymphopoiesis and the Response to Ionizing Irradiation

Susan M. Mendrysa,[1]† Matthew K. McElwee,[1] Jennifer Michalowski,[1]‡ Kathleen A. O'Leary,[1] Karen M. Young,[2] and Mary Ellen Perry[1]*

Department of Oncology, School of Medicine,[1] and Department of Pathobiological Sciences, School of Veterinary Medicine,[2] University of Wisconsin, Madison, Wisconsin 53706

Received 27 August 2002/Returned for modification 23 September 2002/Accepted 13 October 2002

The function of the p53 tumor suppressor protein must be highly regulated because p53 can cause cell death and prevent tumorigenesis. In cultured cells, the $p90^{MDM2}$ protein blocks the transcriptional activation domain of p53 and also stimulates the degradation of p53. Here we provide the first conclusive demonstration that $p90^{MDM2}$ constitutively regulates p53 activity in homeostatic tissues. Mice with a hypomorphic allele of *mdm2* revealed a heretofore unknown role for *mdm2* in lymphopoiesis and epithelial cell survival. Phenotypic analyses revealed that both the transcriptional activation and apoptotic functions of p53 were increased in these mice. However, the level of p53 protein was not coordinately increased, suggesting that $p90^{MDM2}$ can inhibit the transcriptional activation and apoptotic functions of p53 in a manner independent of degradation. Cre-mediated deletion of *mdm2* caused a greater accumulation of p53, demonstrating that $p90^{MDM2}$ constitutively regulates both the activity and the level of p53 in homeostatic tissues. The observation that only a subset of tissues with activated p53 underwent apoptosis indicates that factors other than $p90^{MDM2}$ determine the physiological consequences of p53 activation. Furthermore, reduction of *mdm2* in vivo resulted in radiosensitivity, highlighting the importance of *mdm2* as a potential target for adjuvant cancer therapies.

The *mdm2* gene is essential for murine development unless the *p53* tumor suppressor gene is inactivated (21, 43). *mdm2* was discovered through its amplification on murine double-minute chromosomes (7) and encodes a negative regulator of p53, $p90^{MDM2}$, which inhibits p53 in two genetically distinct ways in cultured cells (28). $p90^{MDM2}$ binds directly to the transcriptional activation domain of p53 and blocks p53-dependent transcription (42, 46, 54). In addition, $p90^{MDM2}$ ubiquitinates p53, stimulating its export from the nucleus (8, 50) as well as its degradation (15, 18, 27). It is not clear which of these inhibitory functions of $p90^{MDM2}$ checks the function of p53 during embryogenesis; however, control of p53 is critical, because p53 can both arrest the cell cycle and induce apoptosis (23, 61).

p53 is critical for preventing tumors in humans and mice (6, 17, 20). However, since activation of p53 can be detrimental to cell survival, the mechanisms controlling the activity of p53 must be exquisitely balanced. In spite of their importance, little is known of the mechanisms that keep the activity of p53 low or undetectable in adult murine tissues (3, 10, 25, 34, 35, 37, 47). p53 protein is expressed in multiple murine tissues, and both its levels and activity are increased in response to whole-body ionizing radiation (40). Although some of the factors that activate p53 in response to DNA damage have been identified, none have been shown to influence the basal level or activity of p53.

In cultured cells, p53 constitutively stimulates expression of *mdm2* (37), thereby determining the level of its own inhibitor, $p90^{MDM2}$. This autoregulatory loop has given rise to a model in which p53 maintains its low basal level and activity by determining the level of $p90^{MDM2}$ (1, 60). Although the p53/MDM2 autoregulatory loop model is appealing, it does not strictly apply to homeostatic tissues. The regulatory interactions between p53 and *mdm2* clearly differ between cultured cells and intact tissues. Whereas p53 constitutively regulates *mdm2* expression in cultured cells, it does not regulate the basal level of *mdm2* expression in vivo (31, 37). However, p53 does stimulate *mdm2* expression following whole-body ionizing radiation, suggesting that the p53/MDM2 autoregulatory loop may operate in vivo under specific conditions (37).

It is not known whether *mdm2* is critical for regulating p53 constitutively in homeostatic tissues. Indirect evidence for a role for $p90^{MDM2}$ in regulating p53 in adult tissues comes from studies of human tumors. In the subset of human tumors lacking inactivating mutations in *p53*, *mdm2* is often overexpressed (30, 45), suggesting that high levels of $p90^{MDM2}$ can substitute for mutation of *p53* and allow tumorigenesis. Indeed, inhibition of $p90^{MDM2}$ expression in cultured human tumor lines activates wild-type p53, indicating that $p90^{MDM2}$ constitutively blocks the activity of p53 in these cells (4). Recently, the physical interaction between p53 and $p90^{MDM2}$ has become the target of adjuvant chemotherapies designed to sensitize human tumors to cancer therapies that rely on activation of p53 for their efficacy (2, 32, 33, 41). The utility of such therapies depends in part on whether $p90^{MDM2}$ is critical for inhibiting p53 in homeostatic tissues. If $p90^{MDM2}$ is critical for maintaining low levels of p53 activity, inhibition of the $p90^{MDM2}$/p53 interaction could induce widespread apoptosis that would be detrimental to the patient.

* Corresponding author. Present address: Cancer Cell Biology Branch, Division of Cancer Biology, National Cancer Institute, Suite 5000, 6130 Executive Blvd., Bethesda, MD 20892-7396. Phone: (301) 496-7028. Fax: (301) 402-1037. E-mail: perryma@mail.nih.gov.

† Present address: Fred Hutchinson Cancer Research Center, Seattle, Wash.

‡ Present address: National Cancer Institute, Bethesda, Md.

To test whether *mdm2* was critical for regulating p53 under homeostatic conditions, we generated a conditionally null allele of *mdm2*. In doing so, we fortuitously generated a hypomorphic allele of *mdm2* (*mdm2*^{puro}) that expresses reduced amounts of *mdm2* mRNA and p90^{MDM2}. Mice carrying one *mdm2*^{puro} allele and a known null allele of *mdm2* are small, lymphopenic, and radiosensitive, with an increased frequency of apoptosis in both lymphocytes and epithelial cells. All of these phenotypes were dependent on p53, demonstrating that p90^{MDM2} does inhibit p53 constitutively in homeostatic tissues. However, although both the transcriptional activation and apoptotic functions of p53 are enhanced in mice expressing reduced levels of *mdm2*, the level of p53 protein is not coordinately increased. These results have important implications for rational approaches to activating p53 in human tumors.

MATERIALS AND METHODS

Generation of targeted ES cells. Constructs containing genomic sequences of *mdm2* from a murine 129/Sv genomic library were obtained from Stephen Jones, University of Massachusetts (21). To generate the targeting vector, a PGKpuro cassette flanked by *loxP* sites was inserted into an *Eco*RI site within *mdm2* intron 6 in the same transcriptional orientation as *mdm2*. An 87-bp fragment containing a third *loxP* site was introduced into a *Hin*cII site within *mdm2* intron 9. The herpes simplex virus thymidine kinase gene was cloned 1.7 kb upstream of *mdm2* exon 7.

129/Sv-derived AB2.2 embryonic stem (ES) cells were electroporated with 30 μg of *Kpn*I-linearized targeting vector DNA and selected in medium containing 3 μg of puromycin (Sigma) per ml and 2 μM ganciclovir 24 h after electroporation. Doubly-resistant ES clones were screened for homologous recombination at the 5′ end of the *mdm2* allele by Southern analysis of *Bam*HI-digested genomic DNA with a 0.7-kb *Bam*HI-*Kpn*I fragment of *mdm2* intron 6 (probe a) external to the targeting vector. ES clones scoring positive were screened by Southern analysis of *Nde*I-digested DNA with a 750-bp fragment of *mdm2* exon 12 (probe c) to detect homologous recombination at the 3′ end of the targeting vector. The presence of the *loxP* site 3′ to *mdm2* exon 9 was confirmed by Southern blot analysis of *Bam*HI-digested DNA with a 500-bp *Hin*cII fragment (probe b) spanning exon 9.

Generation of mice carrying *mdm2*^{puro}, *mdm2*^{flox}, and *mdm2*$^{\Delta 7\text{-}9}$ alleles. The University of Wisconsin Transgenic Animal Facility injected *mdm2*$^{puro/+}$ ES cells into C57BL/6 blastocysts. Chimeric males from two ES cell lines (64 and 125) were used to produce *mdm2*$^{+/puro}$ mice on a mixed C57BL/6 × 129/Sv genetic background as well as an inbred 129/Sv background (Taconic). *mdm2*$^{+/flox}$ and *mdm2*$^{+/\Delta 7\text{-}9}$ mice were created by mating *mdm2*$^{+/puro}$ mice to transgenic mice expressing *Cre* under control of the minimal *rosa26* promoter (*R26-Cre* mice). The *R26-Cre* mice were kindly provided by Eric Sandgren, University of Wisconsin, and have been given the designation TgN(R26cre)15EPS (11). *Mx-Cre* mice were obtained from John Petrini with the kind permission of Klaus Rajewski (29).

Genotyping and maintenance of mice. The *mdm2*^{puro} and *mdm2*$^{+}$ alleles were distinguished with primers 5′-CTGTGTGAGCTGAGGGAGATGTG-3′ and 5′-CCTGGATTTAATCTGCAGCACTC-3′, which yield a 397-bp (*mdm2*^{puro}) and 310-bp (*mdm2*$^{+}$) PCR product, respectively. The *mdm2*^{flox} allele was detected with primers 5′-GTATTGGGCATGTGTTAGACTGG-3′ and 5′-CTTCAGATCACTCCCACCTTC-3′, which yield a 225-bp (*mdm2*^{flox}) and 125-bp (*mdm2*$^{+}$) PCR product, respectively. The *mdm2*$^{\Delta 7\text{-}12}$ allele was detected with primers 5′-GGCAAAGGATGTGATACGTGGAAG-3′ and 5′-CCAGTTTCACTAATGACACAAACATG-3′ in the *hprt* minigene, which yield an 830-bp PCR product. The *mdm2*$^{\Delta 7\text{-}9}$ allele was detected with primers 5′-GTATTGGGCATGTGTTAGACTGG-3′ and 5′-CCTGGATTTAATCTGCAGCACTC-3′, which yield a 240-bp PCR product.

Mice were housed in an American Association for the Accreditation of Laboratory Animal Care-approved facility. The *mdm2*$^{\Delta 7\text{-}12}$ allele (21) was backcrossed to C57BL/6 mice (Jackson Laboratory) for eight to ten generations and also maintained on a mixed 129/Sv × C57BL/6 background. *mdm2*$^{flox/\Delta 7\text{-}12}$ mice were of mixed genetic background (FVB × 129/Sv × C57BL/6) and were compared with their littermates. 129/Sv and C57BL/6 mice carrying a deletion for *p53* (20) were obtained from Paul Lambert (University of Wisconsin). All mice were analyzed at 5 to 6 weeks of age unless otherwise noted.

Conditional deletion of *mdm2*. Upon injection of double-stranded RNA, expression of *cre* can be induced efficiently in the spleen, liver, and thymus of mice carrying the *cre* gene under the control of an interferon-responsive promoter, Mx-1 (29). *mdm2*$^{flox/+}$ mice carrying one *Mx-cre* allele were bred to *mdm2*$^{+/\Delta 7\text{-}12}$ mice to generate *mdm2*$^{flox/\Delta 7\text{-}12}$ *Mx-cre*$^{+}$ mice and controls. Cre expression was induced as described before (29), and 48 h after induction, tissues were isolated. Conversion of the *mdm2*^{flox} allele to the *mdm2*$^{\Delta 7\text{-}9}$ allele was assessed by PCR.

Flow cytometry. Bone marrow cells were flushed from both femurs with phosphate-buffered saline supplemented with 3% fetal bovine serum (PF3). Single-cell suspensions from spleen and thymus were prepared by pressing tissues between frosted-glass microscope slides and dispersing cells in PF3. Contaminating mature erythrocytes were lysed in Gey's solution. Aliquots of 5×10^5 cells were stained with the indicated antibody and appropriate isotype controls. Hematopoietic lineages were identified with fluorescein isothiocyanate-conjugated anti-CD4 (clone GK1.5), phycoerythrin-conjugated anti-CD8 (clone 53-6.7), fluorescein isothiocyanate-conjugated anti-CD45R/B220 (clone RA3-6B2), phycoerythrin-conjugated anti-immunoglobulin M (clone R6-60.2), and phycoerythrin-conjugated anti-CD43 (clone S7) (BD-Pharmingen). Following a 20-min incubation on ice, cells were washed and resuspended in PF3.

To assess apoptosis, 10^6 cells were stained either for CD8, CD4, or B220 as described above. An aliquot of 2×10^5 cells was removed, washed in annexin binding buffer (10 mM HEPES, 140 mM NaCl, and 2.5 mM $CaCl_2$, pH 7.4), and incubated with annexin V (633 conjugate; Molecular Probes) for 15 min at room temperature. The cells were then diluted in cold annexin binding buffer and incubated with propidium iodide. Early apoptotic (annexin positive, propidium iodide negative) cells were counted on a FACSCalibur flow cytometer, and the data were analyzed with Cell Quest software (Becton Dickinson).

Peripheral blood analysis. Peripheral blood was collected from the retroorbital sinus of anesthetized mice and transferred immediately into Microtainer tubes containing dipotassium EDTA (Becton Dickinson). Complete blood counts were performed by the Clinical Pathology Laboratory of the Veterinary Medical Teaching Hospital at the University of Wisconsin School of Veterinary Medicine with an Advia 120 automated hematology analyzer (Bayer). Differential counts were performed manually.

Histology and cytology. Tissues were fixed in 10% neutral buffered formalin, dehydrated, and embedded in paraffin blocks. Apoptosis was assayed by detecting terminal deoxynucleotidyltransferase-mediated dUTP-biotin nick-end labeling (TUNEL)-positive cells with an ApopTag Fluorescein Plus in situ apoptosis detection kit (Intergen), with the following modifications of the recommended protocol. Following incubation with terminal deoxynucleotidyltransferase enzyme, slides were incubated in stop-wash buffer for 30 min at 37°C. After antidigoxigenin conjugate was applied, slides were incubated for 1 h at room temperature. Slides were mounted under glass coverslips with Vectashield antifade mounting medium (Vector) containing 0.5 μg of propidium iodide per ml and visualized on a Bio-Rad MRC 1024 laser scanning confocal microscope at the Keck Biological Imaging Laboratory (University of Wisconsin). For bone marrow differential counts, cells were placed onto glass slides with fine brushes, air dried, and stained with Wright stain.

In vivo radiation sensitivity. At 5 to 6 weeks of age, mice were irradiated with γ rays from a ^{137}cesium source at a dose rate of 3.1 gray (Gy)/min and monitored daily.

Northern analyses. Northern blots were prepared and probed for the glyceraldehyde-3-phosphate dehydrogenase (*gapdh*) and *mdm2* genes as described previously (38). The *p21* probe was a 750-bp *Eco*RI fragment from pCMW35 (a gift from Bert Vogelstein, Johns Hopkins University).

Western analyses. Whole tissues were lysed in radioimmunoprecipitation assay (RIPA) buffer (16) supplemented with the protease inhibitors phenylmethylsulfonyl fluoride, aprotinin, and leupeptin. For the analysis of p90^{MDM2} expression, p90^{MDM2} was immunoprecipitated from 1.5 mg of lysate and detected by Western analysis as described previously (48). For analysis of p53, TATA-binding protein (TBP), and p21 levels, 100 μg of lysates of whole thymuses or spleens were loaded in each lane. Individual thymocytes were isolated as described above, and 2×10^6 cell equivalents were loaded in each lane. p53 was detected with the CM5 polyclonal antiserum (Novocastra), TBP was detected with a monoclonal antibody from Richard Burgess (University of Wisconsin), p21 was detected with monoclonal antibody F-5 (Santa Cruz), and BAX was detected with polyclonal antibody N-20 (Santa Cruz). Secondary antibodies conjugated to horseradish peroxidase were anti-mouse immunoglobulin G (American Qualex) and anti-rabbit immunoglobulin G (Sigma). Signals were detected by enhanced chemiluminescence (Amersham).

Cell cycle analysis of MEFs. Mouse embryo fibroblasts (MEFs) with various *mdm2* genotypes were isolated from 14-day-old embryos and plated in triplicate at a density of 10^6 cells per 10-cm dish at passage 2 (55). Every 3 days, the cells

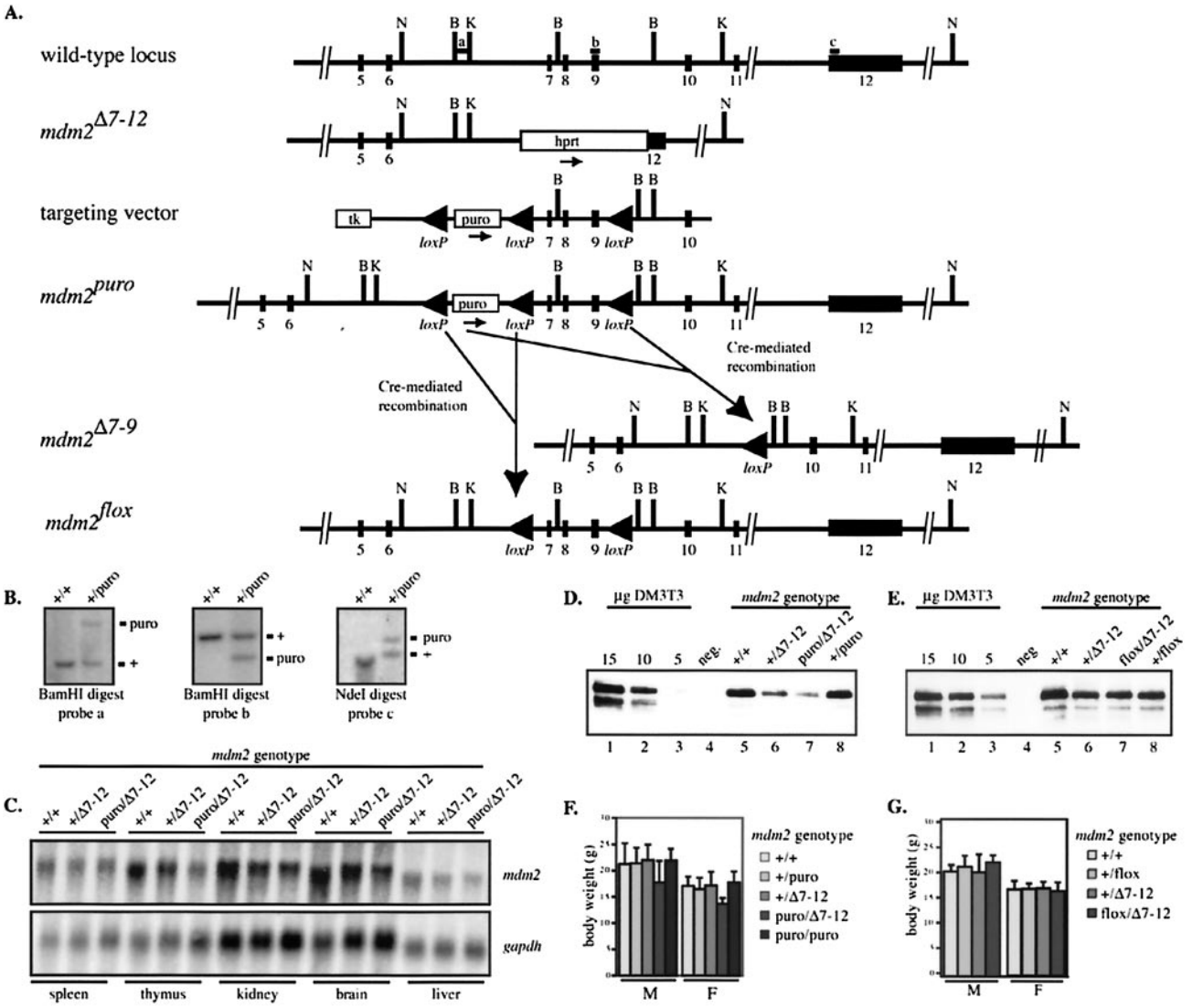

FIG. 1. Generation and characterization of a hypomorphic allele of *mdm2*. (A) Partial structure of murine *mdm2* locus, known null allele ($mdm2^{\Delta 7\text{-}12}$), targeting vector, hypomorphic conditional allele ($mdm2^{puro}$), recombined null allele ($mdm2^{\Delta 7\text{-}9}$), and recombined conditional allele ($mdm2^{flox}$). Abbreviations: *loxP*, Cre recombination site; *hprt*, hypoxanthine phosphoribosyl transferase minigene cassette; puro, puromycin resistance cassette; tk, herpes simplex virus thymidine kinase cassette. N, *Nde*I; B, *Bam*HI; K, *Kpn*I. Probes a, b, and c were used for the experiment shown in panel B. (B) Representative Southern analyses of targeted ES cells. Genomic DNA was digested with *Bam*HI or *Nde*I and probed as indicated. Approximate sizes of fragments from wild-type and targeted alleles were 2.6 and 4.7 kb, respectively (probe a), 1.7 and 1.2 kb, respectively (probe b), and 13.0 and 15.1 kb, respectively (probe c). (C) Northern analysis of *mdm2* mRNA in multiple tissues. *gapdh* mRNA was used as an internal control. (D and E) Immunoprecipitation followed by Western analysis of $p90^{MDM2}$ in testes from (D) $mdm2^{puro/\Delta 7\text{-}12}$ and (E) $mdm2^{flox/\Delta 7\text{-}12}$ mice and respective control mice. Lanes 1 to 3, decreasing amounts of lysate from DM3T3 cells were used as standards. Lane 4, preimmune serum was incubated with lysate from a wild-type testis as a negative control. Lanes 5 to 8, lysates from the testis of mice of the indicated genotypes were incubated with antiserum to MDM2. (F and G) Average 5-week body weights of (F) $mdm2^{puro/\Delta 7\text{-}12}$ and (G) $mdm2^{flox/\Delta 7\text{-}12}$ mice and control mice. The average body weights of 5-week-old $mdm2^{puro/puro}$ mice are included in panel F.

were trypsinized, counted, and replated at the starting density. To determine sensitivity to ionizing irradiation, MEFs were plated at a density of 5×10^5 cells per 6-cm dish and irradiated with either 2 or 8 Gy 24 h after plating. At 16 h following treatment, irradiated and untreated cells were labeled with 10 μM bromodeoxyuridine for 4 h (24). Cells were fixed with 70% ethanol, and nuclei were prepared for staining by established methods (52). The nuclei were stained for 1 h with fluorescein isothiocyanate-conjugated antibromodeoxyuridine antibody (Becton Dickinson), incubated overnight with 0.3 mg of RNase A per ml, and then stained with 50 μg of propidium iodide per ml. Propidium iodide and bromodeoxyuridine incorporation were quantitated on a FACSCalibur flow cytometer.

RESULTS

***mdm2* Gene Targeting.** To generate a conditional allele of *mdm2* ($mdm2^{puro}$), we flanked *mdm2* exons 7 through 9 with Cre recombination (*loxP*) sites (Fig. 1A) (51) so that Cre-mediated recombination would remove three critical coding exons of *mdm2* ($mdm2^{\Delta 7\text{-}9}$). A third *loxP* site was placed 5′ of the puromycin resistance (puro) cassette to allow its removal after targeting. ES cells were electroporated with the targeting

vector, and ES cells surviving selection were screened by Southern analysis (Fig. 1B). Lines of mice from two independently derived $mdm2^{+/puro}$ ES cell clones were established on both a mixed C57BL/6 × 129/Sv and an inbred 129/Sv background, all of which demonstrated the phenotypes reported here.

The functionality of the $mdm2^{puro}$ allele prior to Cre-mediated recombination was assessed by its ability to rescue the embryonic lethality of mice lacking *mdm2*. $mdm2^{+/puro}$ mice were bred to mice carrying one wild-type allele and one known null allele of *mdm2* ($mdm2^{+/\Delta 7\text{-}12}$) (21). Among the progeny of such matings were compound heterozygotes of the genotype $mdm2^{puro/\Delta 7\text{-}12}$, demonstrating that $mdm2^{puro}$ is a functional *mdm2* allele (see below). With a similar genetic approach, we verified that a recombined *mdm2* allele lacking exons 7 to 9 ($mdm2^{\Delta 7\text{-}9}$) was functionally inactive.

By breeding $mdm2^{+/puro}$ mice to *R26-Cre* mice (11), we obtained mice with germ line *mdm2* alleles that had undergone complete recombination ($mdm2^{\Delta 7\text{-}9}$) or had selectively lost the puromycin cassette ($mdm2^{flox}$) (Fig. 1A). Of 137 progeny from matings between $mdm2^{+/\Delta 7\text{-}9}$ and $mdm2^{+/\Delta 7\text{-}12}$ mice, none were of the genotype $mdm2^{\Delta 7\text{-}9/\Delta 7\text{-}12}$, indicating that the $mdm2^{\Delta 7\text{-}9}$ allele cannot rescue the *mdm2* null phenotype ($P < 0.001$). Furthermore, when $mdm2^{+/\Delta 7\text{-}9}$ heterozygotes were interbred, no mice of the genotype $mdm2^{\Delta 7\text{-}9/\Delta 7\text{-}9}$ were born (0 of 160 offspring; $P < 0.001$). These tests indicate that the $mdm2^{\Delta 7\text{-}9}$ allele is nonfunctional. Further testing of the $mdm2^{\Delta 7\text{-}9}$ allele (see below) demonstrated that it was functionally equivalent to the known null allele $mdm2^{\Delta 7\text{-}12}$.

***mdm2*^{puro} is a hypomorphic allele of *mdm2*.** The percentage of $mdm2^{puro/\Delta 7\text{-}12}$ mice obtained from matings between $mdm2^{+/puro}$ and $mdm2^{+/\Delta 7\text{-}12}$ mice was slightly lower than the expected Mendelian frequency of 25%, suggesting that a subset of these mice was dying in utero. This underrepresentation was clearest in female progeny. On mixed and F_1 C57BL/6 × 129/Sv genetic backgrounds, the percentage of female $mdm2^{puro/\Delta 7\text{-}12}$ mice was only 15 and 16%, respectively ($P < 0.05$). The presence of the puromycin resistance cassette accounts for the decreased viability of female $mdm2^{puro/\Delta 7\text{-}12}$ mice, since female $mdm2^{flox/\Delta 7\text{-}12}$ mice, which differ from $mdm2^{puro/\Delta 7\text{-}12}$ mice only by the absence of the puromycin cassette, were born at the expected frequency.

We reasoned that the partially penetrant embryonic lethality observed in $mdm2^{puro/\Delta 7\text{-}12}$ mice might result from interference of the puromycin cassette with *mdm2* expression. Northern analysis revealed that, in all tissues examined, expression of *mdm2* was reduced approximately 50% in $mdm2^{+/\Delta 7\text{-}12}$ mice relative to wild-type mice (Fig. 1C) consistent with a 50% reduction in *mdm2* gene dosage. The level of *mdm2* mRNA in tissues from $mdm2^{puro/\Delta 7\text{-}12}$ mice was further reduced to, on average, 30% of the level in wild-type tissues. Detection of $p90^{MDM2}$ by immunoprecipitation followed by Western analysis demonstrated that $mdm2^{puro/\Delta 7\text{-}12}$ mice also expressed less $p90^{MDM2}$ than wild-type, $mdm2^{+/puro}$, or $mdm2^{+/\Delta 7\text{-}12}$ mice in the testis (Fig. 1D), thymus, spleen, and brain (data not shown). Decreased expression of $p90^{MDM2}$ in $mdm2^{puro/\Delta 7\text{-}12}$ tissues was dependent on the puromycin cassette, as the levels of $p90^{MDM2}$ in tissues from $mdm2^{flox/\Delta 7\text{-}12}$ mice and $mdm2^{+/\Delta 7\text{-}12}$ mice were equivalent (Fig. 1E). Thus, the puromycin cassette reduces expression of *mdm2* and $p90^{MDM2}$ in multiple adult tissues.

TABLE 1. Comparison of wet weights of tissues from age-matched wild-type and $mdm2^{puro/\Delta 7\text{–}12}$ mice[a]

Tissue	Age (wk)	Ratio, $mdm2^{puro/\Delta 7\text{–}12}/mdm2^{+/+}$	
		Males	Females
Kidney	10	0.8 ± 0.2 (0.01)	0.8 ± 0.1 (0.06)
Liver	10	0.9 ± 0.2 (0.34)	0.6 ± 0.2 (0.02)
Spleen	10	0.7 ± 0.3 (0.02)	0.4 ± 0.1 (0.02)
Thymus	5	0.4 ± 0.1 (<0.001)	0.4 ± 0.1 (0.001)

[a] Presented as the ratio of the average weight ± standard deviation (*P*).

Together, these data demonstrate that the $mdm2^{puro}$ allele is hypomorphic, whereas the $mdm2^{flox}$ allele is functionally wild type. The low level of *mdm2* expression in $mdm2^{puro/\Delta 7\text{-}12}$ mice allowed us to perform a comprehensive analysis of the physiological functions of *mdm2* because it eliminated the need to select tissues for Cre expression. In characterizing the $mdm2^{puro/\Delta 7\text{-}12}$ mice, we determined that *mdm2* regulates the activity of p53 in homeostatic tissues.

Decreased body weight in $mdm2^{puro/\Delta 7\text{-}12}$ mice. Viable $mdm2^{puro/\Delta 7\text{-}12}$ mice developed normally, with no increase in lethality upon weaning. At five weeks of age, a 15 to 20% reduction in body weight was evident in both male and female $mdm2^{puro/\Delta 7\text{-}12}$ mice compared with wild-type mice (Fig. 1F). In contrast, age-matched $mdm2^{puro/puro}$ mice (Fig. 1F) and $mdm2^{flox/\Delta 7\text{-}12}$ mice (Fig. 1G) were comparable in weight to wild-type mice, demonstrating that normal body weight is dependent on the level of *mdm2* expression. All organs examined were smaller in both male and female $mdm2^{puro/\Delta 7\text{-}12}$ mice than in wild-type mice, with the most dramatic reductions in the lymphoid organs (Table 1). Histological analyses of the liver, kidney, and intestines failed to reveal any obvious defects that could account for the reduction in body weight. The decrease in both body weight and organ size were also seen in $mdm2^{puro/\Delta 7\text{-}9}$ mice, indicating that our new deleted allele is functionally similar to the known $mdm2^{\Delta 7\text{-}12}$ allele.

***mdm2*$^{puro/\Delta 7\text{-}12}$ mice exhibit defects in multiple hematopoietic lineages.** Complete blood count analysis of peripheral blood revealed a mild anemia in $mdm2^{puro/\Delta 7\text{-}12}$ mice, which had a red blood cell count that was 82% of that of wild-type mice (Table 2). The white blood cell count in $mdm2^{puro/\Delta 7\text{-}12}$ mice was only 30% of the wild-type count. This dramatic reduction in white blood cells was paralleled by a decrease in the concentration of lymphocytes to 37% of that of wild-type mice. In contrast, the concentration of neutrophils was 60% of the wild-type value, suggesting that the deficiency in white blood cells is largely due to a decrease in lymphocytes.

The spleen, thymus, and bone marrow of $mdm2^{puro/\Delta 7\text{-}12}$ mice also showed decreases in the number of lymphoid cells (Fig. 2A to C). The spleens of $mdm2^{puro/\Delta 7\text{-}12}$ mice contained, on average, 34% of the number of cells in spleens from wild-type mice (Fig. 2D). Flow cytometric analysis indicated the number of T cells in $mdm2^{puro/\Delta 7\text{-}12}$ mice was reduced to 40% of that in the wild type, whereas the B cells were reduced to 15% (Fig. 2D). Thus, decreased splenic cellularity of $mdm2^{puro/\Delta 7\text{-}12}$ mice is attributed to deficits in both T and B lymphocytes stemming from a subphysiological level of *mdm2*.

TABLE 2. Hematological profiles of age-matched wild-type and *mdm2*$^{puro/\Delta 7–12}$ mice[a]

mdm2 genotype	No.	RBC (10^6/μl)	WBC (10^3/μl)	Neutrophils (10^3/μl)	Lymphocytes (10^3/μl)
+/+	6	8.2 (7.2–9.5)	5.4 (3.5–7.3)	0.5 (0.1–1.0)	3.0 (2.7–3.4)
puro/Δ7–12	5	6.7 (6.3–7.5)	1.6 (1.1–1.8)	0.3 (0.1–0.4)	1.1 (0.8–1.3)

[a] Total red blood cell (RBC) counts and total white blood cell (WBC) counts were determined with an Advia 120 automated hematology analyzer (Bayer). Total neutrophil and lymphocyte counts were calculated from the percentage of these leukocytes (manual differential count) and the total WBC count and are expressed as the average concentration (range).

Consistent with the dramatic reduction in thymus weight, *mdm2* was also determined to be critical for thymocyte development. The thymi of *mdm2*$^{puro/\Delta 7\text{-}12}$ mice were hypocellular (Fig. 2B), containing on average 5% of the number of thymocytes present in wild-type mice (Fig. 2F). During T-cell development, thymocytes progress from a $CD4^-$ $CD8^-$ double-negative stage to a $CD4^+$ $CD8^+$ double-positive stage and then to either a $CD4^+$ or a $CD8^+$ single-positive stage (19). Flow cytometric analysis with CD4 and CD8 markers revealed a significant reduction in the absolute number of thymocytes in all differentiation stages in *mdm2*$^{puro/\Delta 7\text{-}12}$ mice (Fig. 2E and F). The relative proportion of double-positive thymocytes was decreased 20 to 40% compared with wild-type mice (Fig. 2F), suggesting either a partial block in thymocyte maturation from the double-negative to double-positive stage or decreased survival of double-positive cells. However, the decreased cellularity of *mdm2*$^{puro/\Delta 7\text{-}12}$ thymuses cannot be attributed solely to a block in thymocyte development because the absolute number of the least mature, double-negative thymocytes was reduced by greater than 80% from the number in wild-type animals. Together, these results suggest that *mdm2* may play a critical role in T-cell development at multiple stages.

Given that both early T-cell precursors and B cells originate in the bone marrow, the decrease in lymphocytes in the thymuses and spleens of *mdm2*$^{puro/\Delta 7\text{-}12}$ mice could arise from a deficiency in bone marrow lymphocytes. *mdm2*$^{puro/\Delta 7\text{-}12}$ mice contained only half as many bone marrow cells as wild-type mice (Fig. 2G), with a sevenfold decrease in the number of

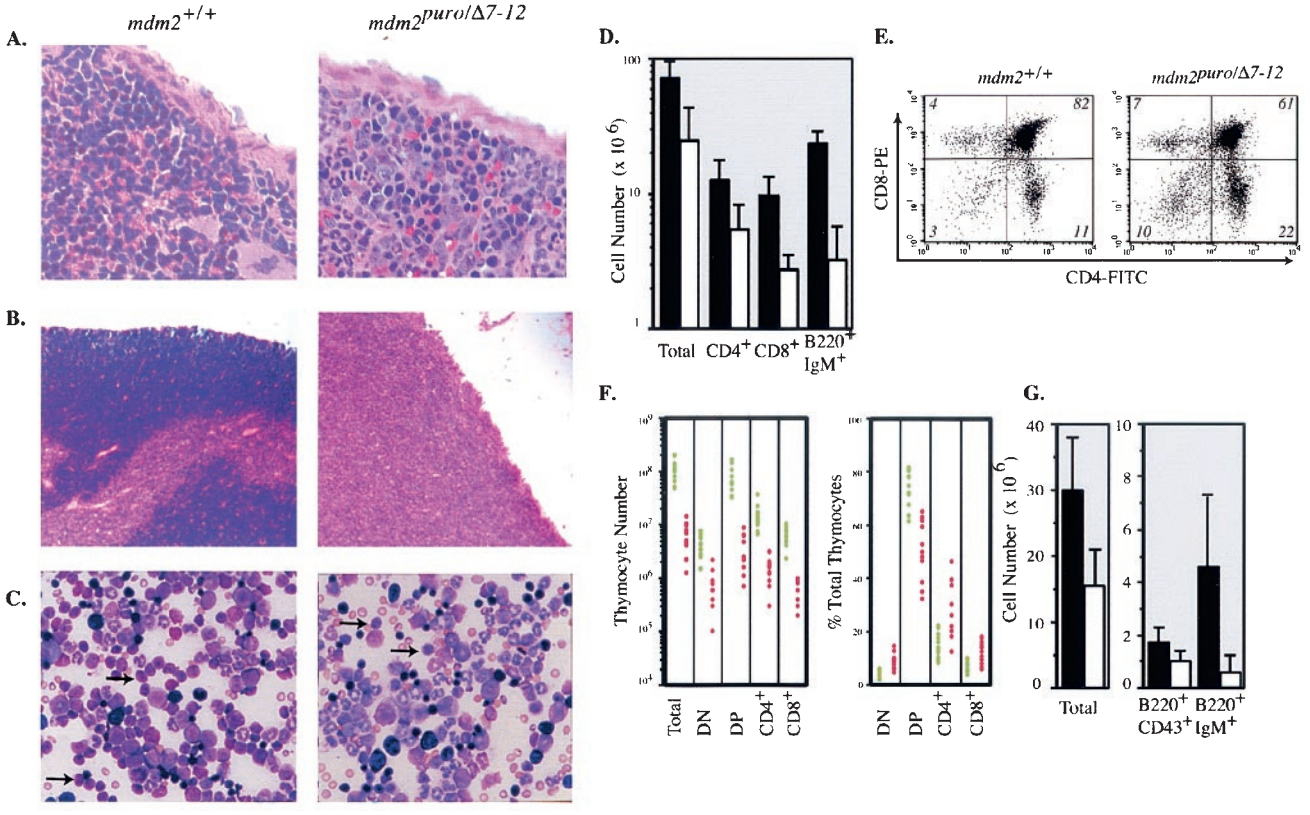

FIG. 2. Lymphopoietic defects in *mdm2*$^{puro/\Delta 7\text{-}12}$ mice. (A and B) Hematoxylin- and eosin-stained 5-μm sections of (A) spleen and (B) thymus from wild-type and *mdm2*$^{puro/\Delta 7\text{-}12}$ mice. (C) Wright-stained bone marrow from *mdm2* wild-type and *mdm2*$^{puro/\Delta 7\text{-}12}$ mice. Lymphocytes are indicated by arrows. (D) Number of total cells, $CD4^+$ and $CD8^+$ T cells, and $B220^+$ IgM^+ B cells in the spleen. Black bars, wild type; white bars, *mdm2*$^{puro/\Delta 7\text{-}12}$. (E) Representative flow cytometric analysis of thymocytes isolated from *mdm2*$^{+/+}$ and *mdm2*$^{puro/\Delta 7\text{-}12}$ mice. (F) Number and percentage of thymocytes in each maturation stage. Each circle represents an individual animal. Green, wild type; red, *mdm2*$^{puro/\Delta 7\text{-}12}$. (G) Average number of total, $B220^+$ $CD43^+$, and $B220^+$ IgM^+ bone marrow cells per two femurs. Black bars, wild type ($n = 12$); white bars, *mdm2*$^{puro/\Delta 7\text{-}12}$ ($n = 12$).

lymphocytes (Fig. 2C). As in the blood, this profound decrease in the number of lymphocytes was accompanied by smaller decreases in other hematopoietic lineages. Both a twofold decrease in the number of erythroid cells, consistent with the mild anemia identified by complete blood count analysis, and a 1.2-fold decrease in the number of granulocytic cells support the conclusion that the hematopoietic defects in *mdm2*$^{puro/\Delta 7\text{-}12}$ mice are most severe in the lymphoid lineage.

Next we assessed whether the deficiency of B lymphocytes could be due to a defect in maturation. Immature progenitor B cells express the CD43 and B220 (CD45R) surface markers, whereas, after the transition from pro-B to pre-B, B cells downregulate CD43 (53, 59). Following the synthesis of μ light chains, B cells express surface IgM and higher levels of B220 (53). Flow cytometric analysis revealed a 40% reduction in the number of B220$^+$ CD43$^+$ immature B cells in the bone marrow of *mdm2*$^{puro/\Delta 7\text{-}12}$ mice compared with wild-type mice, with a further reduction (87%) in the number of more mature, B220$^+$ IgM$^+$ B cells (Fig. 2G). Therefore, as with thymocytes, loss of *mdm2* may interfere with B-cell development at multiple stages, with the reduction in the number of B220$^+$ IgM$^+$ B cells stemming from both a decrease in the number of progenitor cells and a defect in maturation.

Increased p53-dependent apoptosis in *mdm2*$^{puro/\Delta 7\text{-}12}$ lymphocytes. Because p90^{MDM2} can inhibit the apoptotic function of p53 in cultured cells (14), we predicted that the lymphoid deficiencies in *mdm2*$^{puro/\Delta 7\text{-}12}$ mice were due to an increase in the apoptotic activity of p53. We therefore determined the number of apoptotic T and B cells in the thymus and bone marrow, respectively. Costaining for T-cell markers and annexin V, a marker of early stages of apoptosis, revealed a 4.1-fold increase in the percentage of apoptotic double-positive thymocytes, which likely explains the relative paucity of the double-positive population. Increased apoptosis did not strictly coincide with T-cell development, however, as thymocytes of all maturation stages, including the least mature, double-negative cells, showed at least a twofold-greater proportion of annexin V-positive cells (Fig. 3A).

Analysis of the number of apoptotic thymocytes in *mdm2*$^{puro/\Delta 7\text{-}12}$ mice that were homozygous for a null allele of *p53* (20) showed wild-type levels of apoptosis (Fig. 3A), demonstrating that decreased expression of *mdm2* can result in p53-dependent apoptosis. Increased p53 function appears to account for the thymic defects, since *mdm2*$^{puro/\Delta 7\text{-}12}$ mice lacking p53 had thymuses of normal size (Fig. 3B).

Costaining for B220 and annexin V also revealed a 1.9-fold increase in the percentage of apoptotic B cells in the bone marrow of *mdm2*$^{puro/\Delta 7\text{-}12}$ mice relative to wild-type bone marrow (Fig. 3A). B cells from *mdm2*$^{puro/\Delta 7\text{-}12}$ mice lacking p53 showed wild-type levels of apoptosis, and the number of B220$^+$ B cells in the bone marrow of *mdm2*$^{puro/\Delta 7\text{-}12}$ mice was rescued by loss of p53 (Fig. 3C). Together, these results demonstrate that *mdm2* expression is critical for the inhibition of p53-mediated apoptosis during lymphopoiesis.

Increased transactivation function of p53 correlates with decreased *mdm2* expression. Based on our finding that a 70% decrease in *mdm2* expression was sufficient to allow an increase in the apoptotic function of p53, we predicted that the transcriptional activation function of p53 would also be increased in *mdm2*$^{puro/\Delta 7\text{-}12}$ mice. Northern analysis of the p53-responsive gene *p21* revealed that, in both lymphoid and nonlymphoid tissues from *mdm2*$^{puro/\Delta 7\text{-}12}$ mice, expression of *p21* was increased relative to that of the control, *gapdh* (Fig. 4A). The greatest increase in *p21* expression (an average of 10-fold) was found in the spleen, whereas only a 2-fold increase was seen in the thymus. An increase in *p21* expression was also evident in all tissues examined from *mdm2*$^{+/\Delta 7\text{-}12}$ mice, suggesting haploinsufficiency at the *mdm2* locus. The increase in

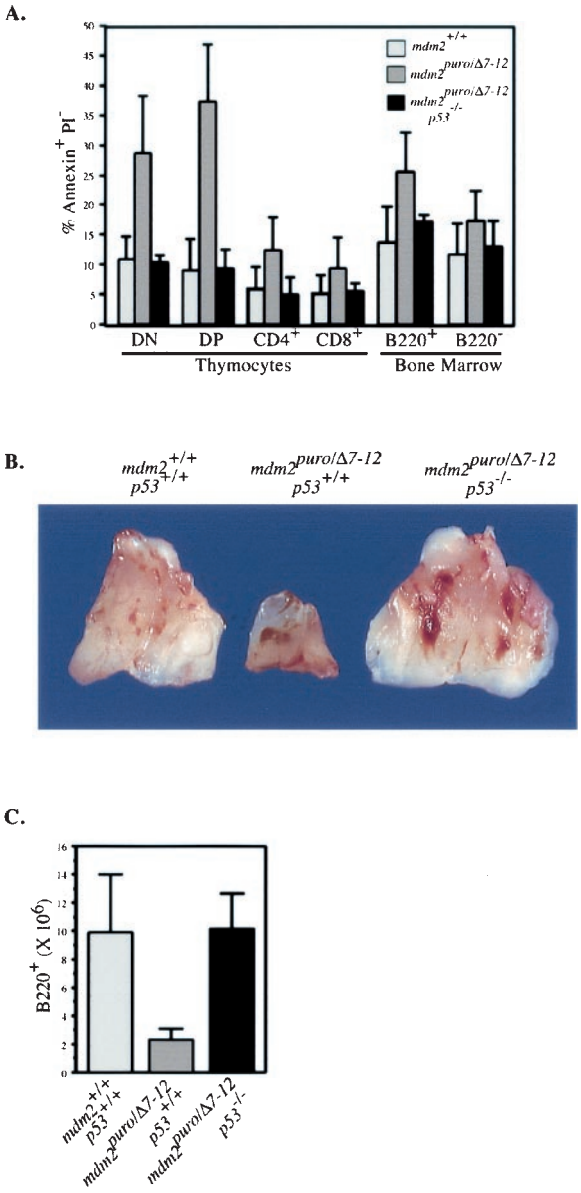

FIG. 3. p53 deficiency rescues lymphopoietic defects in *mdm2*$^{puro/\Delta 7\text{-}12}$ mice. (A) Percentage of apoptotic cells in the lymphoid compartment of wild-type, *mdm2*$^{puro/\Delta 7\text{-}12}$, and *mdm2*$^{puro/\Delta 7\text{-}12}$ *p53*$^{-/-}$ mice. Freshly isolated bone marrow and thymocytes were stained for the indicated B- and T-cell markers, respectively, incubated with annexin V and propidium iodide (PI), and analyzed by flow cytometry. DN, double negative; DP, double positive. (B) Thymuses from wild-type, *mdm2*$^{puro/\Delta 7\text{-}12}$, and *mdm2*$^{puro/\Delta 7\text{-}12}$ *p53*$^{-/-}$ mice. (C) Average number of B220$^+$ bone marrow cells per two femurs from wild-type, *mdm2*$^{puro/\Delta 7\text{-}12}$, and *mdm2*$^{puro/\Delta 7\text{-}12}$ *p53*$^{-/-}$ mice.

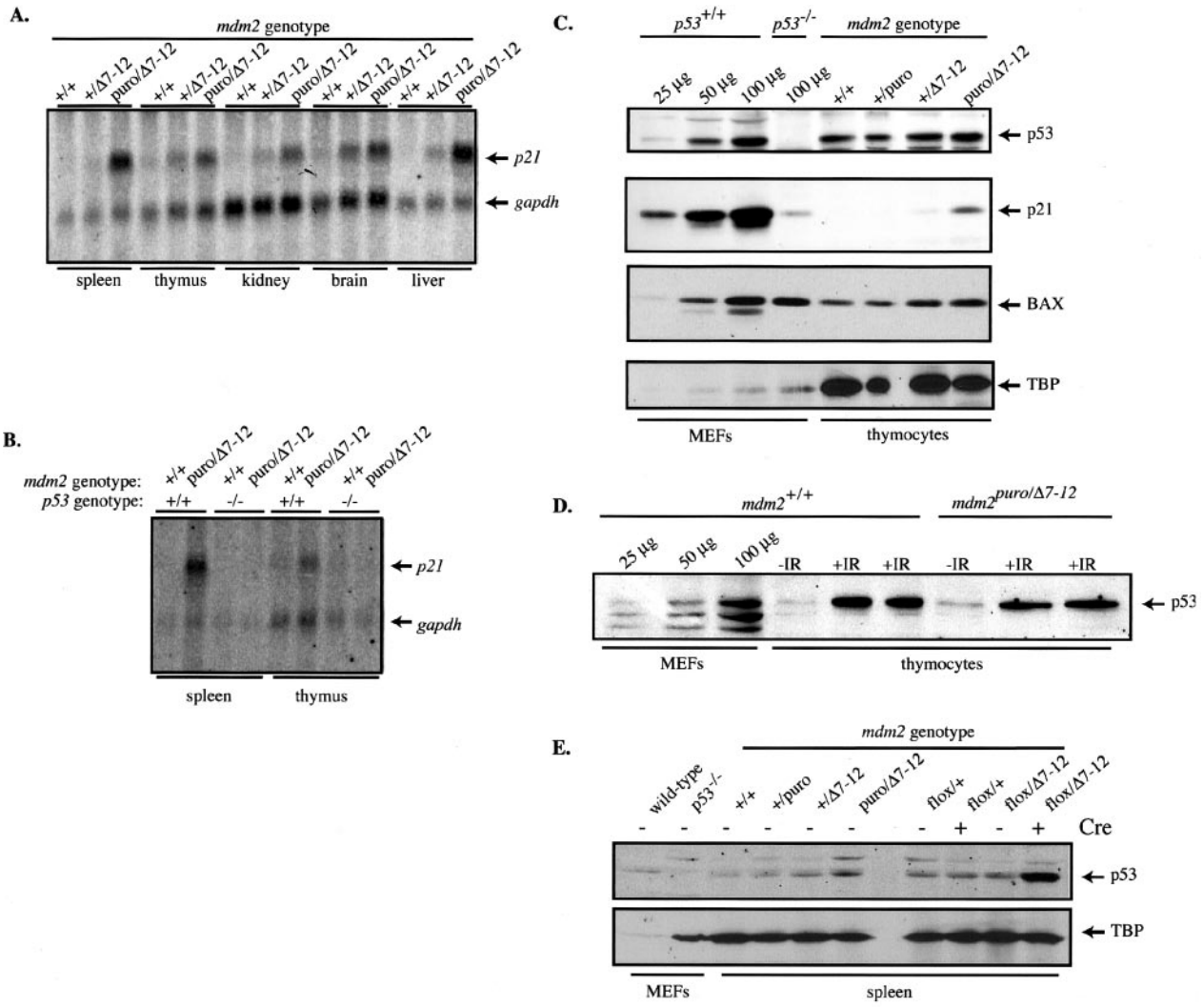

FIG. 4. p53 function is increased independently of p53 accumulation in *mdm2*$^{puro/\Delta 7\text{-}12}$ thymocytes. (A) Northern analysis of *p21* and *gapdh* mRNAs in multiple tissues. (B) Northern analysis of *p21* and *gapdh* mRNAs in the spleen and thymus in the presence and absence of p53. (C) Western analysis of p53, p21, and BAX in isolated thymocytes. MEFs lacking p53 were used as the negative control. TBP was used as a loading control, and increasing amounts of lysate from wild-type MEFs were used as standards. (D) Western analysis of p53 prior to and following DNA damage. Mice were left unirradiated (−IR) or subjected in duplicate to 10 Gy of ionizing radiation (+IR). Four hours after irradiation, thymocytes were isolated. Increasing amounts of lysate from wild-type MEFs were used as standards. (E) Western analysis of p53 following deletion of exons 7 through 9 of *mdm2* in spleens of *mdm2*$^{flox/\Delta 7\text{-}12}$ *Mx-cre*$^{+}$ mice.

p21 mRNA was dependent on the presence of p53, since *mdm2*$^{puro/\Delta 7\text{-}12}$ mice lacking p53 showed wild-type levels of *p21* expression in both spleen and thymus (Fig. 4B). This is the first demonstration that *mdm2* constitutively regulates the transactivation as well as the apoptotic function of p53 in homeostatic tissues.

Increased p53 activity in *mdm2*$^{puro/\Delta 7\text{-}12}$ tissues occurs without a concomitant increase in the level of p53. To determine whether the decreased level of p90^{MDM2} in *mdm2*$^{puro/\Delta 7\text{-}12}$ mice allowed the level of p53 protein to increase, we performed Western analyses of p53. Instead of increasing, the level of p53 decreased in lysates from *mdm2*$^{puro/\Delta 7\text{-}12}$ thymi compared to wild-type thymuses when equivalent amounts of total protein were analyzed (data not shown). The level of the loading control, TBP, was also decreased in lysates from *mdm2*$^{puro/\Delta 7\text{-}12}$ mice, leading us to speculate that nuclear proteins were underrepresented in the samples. As the number of T cells was diminished 10-fold in *mdm2*$^{puro/\Delta 7\text{-}12}$ thymuses, whereas the total thymus weight was decreased only 2.5-fold, a greater proportion of the total protein is likely to be stromal, causing a disproportionate representation of extracellular matrix proteins in lysates of whole thymuses. Thus, we tested whether the level of p53 was increased in preparations of *mdm2*$^{puro/\Delta 7\text{-}12}$ thymocytes isolated identically to those used for the apoptosis assays that showed an increase in p53 function.

Although TBP levels were identical in isolated wild-type and *mdm2*$^{puro/\Delta 7\text{-}12}$ thymocytes, there was no significant increase in the level of p53 protein (Fig. 4C). However, the same blot showed an increase in p21 protein (Fig. 4C) consistent with the

p53-dependent increase in *p21* mRNA shown in whole thymuses, suggesting that the specific activity of p53 was elevated in *mdm2*$^{puro/\Delta 7\text{-}12}$ thymocytes. In contrast, there was no increase in the proapoptotic BAX protein, suggesting that expression of a subset of p53 target genes was increased (Fig. 4C). Indeed, Northern analysis showed no increase in *bax* mRNA in thymuses from *mdm2*$^{puro/\Delta 7\text{-}12}$ mice (data not shown). The increase in p53 function does not appear to be due to a decrease in the shuttling function of p90^{MDM2}, because there was no significant increase in the level of p53 in the nuclei of *mdm2*$^{puro/\Delta 7\text{-}12}$ thymocytes (data not shown).

To verify that our detection method could detect an increase in the level of endogenous p53, we compared the level of p53 in thymocytes from untreated and irradiated wild-type and *mdm2*$^{puro/\Delta 7\text{-}12}$ mice, because whole-body ionizing radiation is known to increase the level of p53 in this cell type (40). The levels of p53 were clearly increased in thymocytes from both *mdm2*$^{puro/\Delta 7\text{-}12}$ and wild-type mice following irradiation (Fig. 4D). Together, these results suggest that, in homeostatic tissues, p90^{MDM2} selectively regulates the specific activity of p53 so that the function but not the stability of p53 is increased in *mdm2*$^{puro/\Delta 7\text{-}12}$ tissues. In contrast to the thymi, the spleens of *mdm2*$^{puro/\Delta 7\text{-}12}$ mice showed a slight increase in the level of p53 (Fig. 4E). However, the increase was much smaller than the 10-fold increase in the expression of *p21* mRNA (Fig. 4B), again indicating that the specific activity of p53 is elevated in *mdm2*$^{puro/\Delta 7\text{-}12}$ tissues.

The increase in the level of p53 was magnified in spleens from *mdm2*$^{flox/\Delta 7\text{-}12}$ *Mx-cre* mice, from which *mdm2* had been conditionally deleted (see Materials and Methods), suggesting that the level of p90^{MDM2} in spleens from *mdm2*$^{puro/\Delta 7\text{-}12}$ mice may be sufficiently high to allow some ubiquitination of p53 (Fig. 4E). Together, these results indicate that although p90^{MDM2} can regulate both p53 function and stabilization in vivo, these two activities of p90^{MDM2} may be independently controlled, as in some tissues stabilization of p53 does not appear to be a prerequisite for increased function.

Spontaneous apoptosis in the small but not large intestine of *mdm2*$^{puro/\Delta 7\text{-}12}$ mice. Given that the transcriptional activity of p53 was increased in all *mdm2*$^{puro/\Delta 7\text{-}12}$ tissues examined, we next investigated whether cell types in addition to lymphocytes showed an increased frequency of p53-dependent apoptosis. Terminal deoxynucleotidyltransferase-mediated dUTP-biotin nick-end labeling (TUNEL), an assay for apoptotic cells (9), revealed no increase in apoptosis in the liver, kidney, or colon of *mdm2*$^{puro/\Delta 7\text{-}12}$ mice (data not shown). In contrast, there was a pronounced, 17-fold increase in the frequency of spontaneous apoptosis in the small intestine (Fig. 5A and B). Most of the apoptotic cells in the small intestines of *mdm2*$^{puro/\Delta 7\text{-}12}$ mice were in the crypts rather than the villi (Fig. 5D), in the same region as the proliferating transitional cells known to undergo p53-mediated apoptosis in response to ionizing radiation (39). The increased incidence of apoptosis in the small intestines of *mdm2*$^{puro/\Delta 7\text{-}12}$ mice was dependent on p53, as loss of p53 abrogated the increased number of apoptotic cells (Fig. 5C). Thus, in addition to lymphocytes, the level of p90^{MDM2} is important for regulation of the apoptotic function of p53 in the epithelial cells of the small intestine.

Growth arrest in *mdm2*$^{puro/\Delta 7\text{-}12}$ mouse embryo fibroblasts.

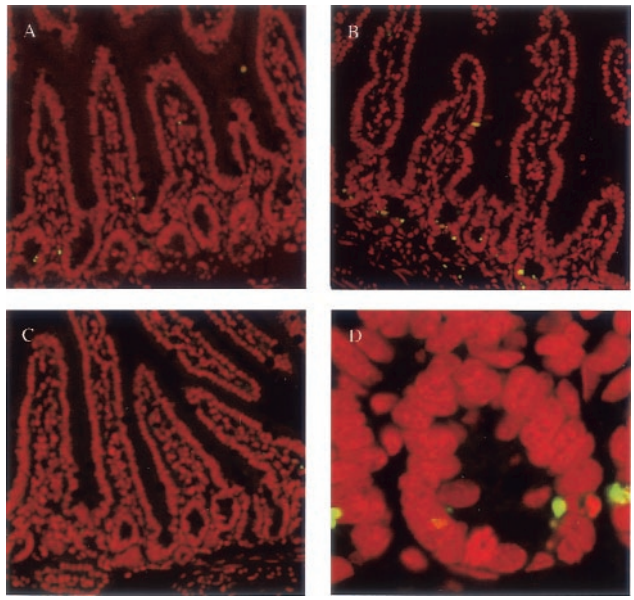

FIG. 5. Increased number of apoptotic cells in crypts of small intestines from *mdm2*$^{puro/\Delta 7\text{-}12}$ mice. TUNEL staining (green) was performed on 5-μm sections of the small intestine. Propidium iodide (red) was used to stain all nuclei. (A) Wild type. (B) *mdm2*$^{puro/\Delta 7\text{-}12}$. (C) *mdm2*$^{puro/\Delta 7\text{-}12}$ *p53*$^{-/-}$. (D) Close-up of crypt from *mdm2*$^{puro/\Delta 7\text{-}12}$ mouse small intestine.

In addition to stimulating apoptosis, p53 can mediate growth arrest in the G_1 phase of the cell cycle (13, 23). To assess whether the reduction in *mdm2* could contribute to a growth arrest, we measured the proliferation rates of mouse embryo fibroblasts (MEFs) from wild-type, *mdm2*$^{+/puro}$, *mdm2*$^{+/\Delta 7\text{-}12}$, and *mdm2*$^{puro/\Delta 7\text{-}12}$ mice. The rate of proliferation correlated with the level of *mdm2*, with MEFs from *mdm2*$^{puro/\Delta 7\text{-}12}$ mice being the slowest to proliferate (Fig. 6A). Moreover, the fraction of cells traversing S phase, as determined by bromodeoxyuridine incorporation, correlated directly with the level of *mdm2* expression. For example, the S-phase fraction of *mdm2*$^{puro/\Delta 7\text{-}12}$ MEFs was 72% ± 4% of that of wild-type MEFs (data not shown), suggesting that the low level of *mdm2* leads to an increase in the G_1 arrest function of p53. This result was consistent with the finding that ionizing radiation, which is known to enhance the G_1 checkpoint function of p53 (24, 32), caused a decrease in the S-phase fraction that correlated inversely with the level of *mdm2* (Fig. 6B). Thus, the level of *mdm2* appears to regulate the G_1 checkpoint function of p53.

Level of *mdm2* expression is a strong determinant of radiation sensitivity in vivo. The increased sensitivity of *mdm2*$^{puro/\Delta 7\text{-}12}$ MEFs to ionizing radiation suggested that the low level of *mdm2* in *mdm2*$^{puro/\Delta 7\text{-}12}$ mice may become critical in response to stress. Therefore, we asked whether *mdm2*$^{puro/\Delta 7\text{-}12}$ mice were more sensitive than wild-type mice to whole-body ionizing radiation. At a dose of 10 Gy, 50% of wild-type mice died between days 12 and 22 posttreatment (Fig. 7), with the remainder surviving the course of the experiment (40 days). In contrast, 100% of *mdm2*$^{puro/\Delta 7\text{-}12}$ mice died between 7 and 9 days posttreatment. Both *mdm2*$^{+/puro}$ and *mdm2*$^{+/\Delta 7\text{-}12}$ mice were also more radiosensitive than wild-

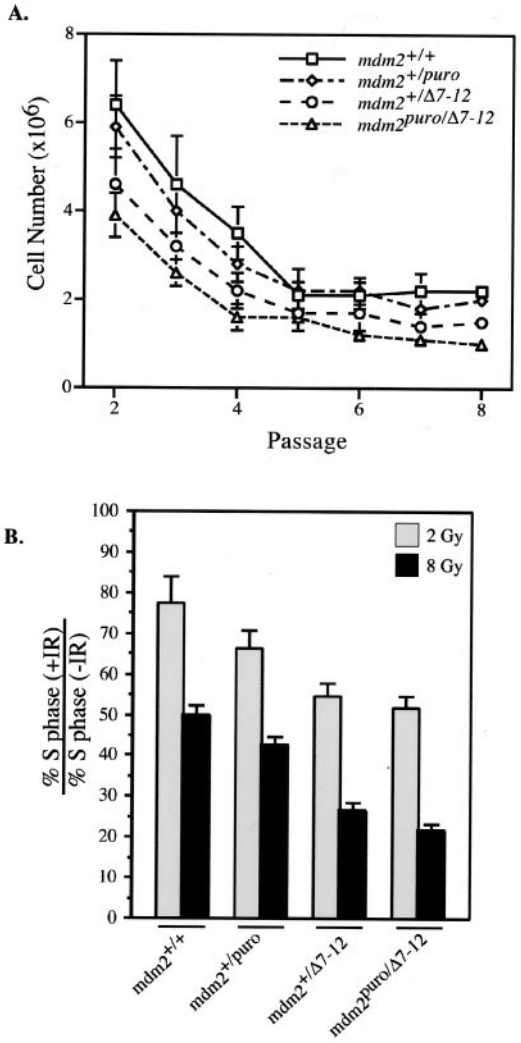

FIG. 6. Proliferative capacity of MEFs from mice of various *mdm2* genotypes. (A) Growth curves for MEFs of the indicated genotypes. MEFs were seeded in triplicate at an initial density of 10^6 cells per plate and counted every 3 days, after which they were replated at the original density. Graphed is the average number of cells per plate at each passage. Consistent results were obtained for independently derived MEFs. (B) Ratio of the percentage of cells in S phase 16 h following treatment with 2 or 8 Gy of ionizing radiation (+IR) to the percentage in S phase in the absence of treatment (−IR). Bromodeoxyuridine incorporation was used to determine the S-phase fraction.

type mice, with 100% of $mdm2^{+/puro}$ and $mdm2^{+/\Delta 7\text{-}12}$ mice dying by days 20 and 14, respectively, following treatment.

Pairwise comparisons with the log-rank test indicate that the survival times of all genotype combinations except $mdm2^{+/puro}$ and $mdm2^{+/\Delta 7\text{-}12}$ are significantly different ($P < 0.005$). The increased sensitivity of $mdm2^{+/puro}$ mice indicates that even a moderate, approximately 20% reduction in *mdm2* is sufficient to sensitize mice to the lethal effects of ionizing radiation. Furthermore, since all the $mdm2^{puro/\Delta 7\text{-}12}$ mice died before any $mdm2^{+/\Delta 7\text{-}12}$ mice died, *mdm2* expression and activity must be exquisitely controlled in vivo, as *mdm2* expression differed by less than twofold between these genotypes. As p53 is a key mediator of radiation-induced death in vivo (58), the increased

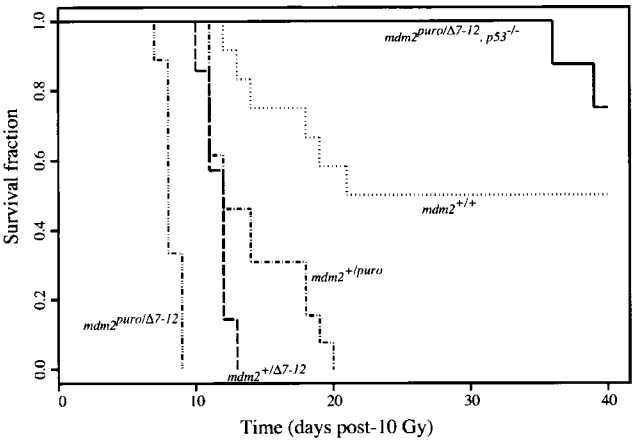

FIG. 7. p53-dependent radiosensitivity in $mdm2^{puro/\Delta 7\text{-}12}$ mice. Kaplan-Meier survival curves of age-matched wild-type ($n = 12$), $mdm2^{puro/\Delta 7\text{-}12}$ ($n = 13$), $mdm2^{+/\Delta 7\text{-}12}$ ($n = 7$), $mdm2^{puro/\Delta 7\text{-}12}$ ($n = 9$), and $mdm2^{puro/\Delta 7\text{-}12}$ $p53^{-/-}$ ($n = 8$) mice following exposure to 10 Gy of whole-body ionizing radiation.

radiation sensitivity in mice with reduced *mdm2* is likely due to aberrant p53 activity stemming from insufficient inhibition of p53 by $p90^{MDM2}$. Indeed, the sensitivity of $mdm2^{puro/\Delta 7\text{-}12}$ mice to whole-body irradiation was dependent on p53, as 100% of $mdm2^{puro/\Delta 7\text{-}12}$ $p53^{-/-}$ mice survived for at least 35 days following irradiation (Fig. 7). Thus, *mdm2* protects mice from the lethal effects of ionizing radiation. These studies identify *mdm2* as a key determinant of radiation sensitivity in vivo.

DISCUSSION

***mdm2* is a survival factor in the thymus, bone marrow, and small intestine.** Mice with decreased expression of *mdm2* have defects in lymphopoiesis and in epithelial cell survival that can be attributed to an increased frequency of spontaneous p53-dependent apoptosis. While all of the phenotypes reported here are dependent on p53, demonstrating that the major role of *mdm2* in adult tissues is to inhibit the activity of p53, our results do not exclude p53-independent functions for $p90^{MDM2}$. Indeed, decreased expression of *mdm2* alters the tumor spectrum in p53-null mice (36). However, to date, no p53-independent phenotypes have been observed in the $mdm2^{puro/\Delta 7\text{-}12}$ mice.

Does $p90^{MDM2}$ block a signal to p53? Tissue-specific differences in susceptibility to p53-mediated apoptosis are not understood. Based on a strong correlation between tissues that accumulate high levels of p53 and those that undergo p53-mediated apoptosis following whole-body ionizing radiation, a model was proposed in which the induced level of p53 protein determines whether a cell type undergoes p53-mediated apoptosis (25, 26, 34). As we have demonstrated, a detectable increase in the level of p53 is not required to stimulate p53-mediated apoptosis in vivo, at least in thymocytes, which show an increased incidence of apoptosis in $mdm2^{puro/\Delta 7\text{-}12}$ mice without an evident rise in the level of p53 protein. These results indicate that the tissue-specific differences in propensity to undergo p53-mediated apoptosis cannot be explained by differences in the accumulation of p53 protein.

Recent evidence suggests that specific covalent modifications alter the ability of p53 to induce apoptosis, and a two-step model has been put forth in which p53 is released from $p90^{MDM2}$ to become stable and also covalently modified to become active (57). Our data indicate that accumulation of p53 is not critical for increased apoptosis. However, in *mdm2*$^{puro/\Delta 7\text{-}12}$ mice, the decrease in *mdm2* expression was sufficient to allow p53-dependent apoptosis in a subset of tissues, suggesting either that p53 is modified constitutively in lymphocytes and epithelial cells of the small intestine or that modification is not required for p53 to stimulate apoptosis. The mice described here will be valuable tools for deciphering which modifications of p53, if any, are required for its apoptotic function.

If modification of p53 is required for spontaneous apoptosis in *mdm2*$^{puro/\Delta 7\text{-}12}$ tissues, it is not evident what signaling pathway mediates the modification. Although aberrant double-strand breaks are known to activate p53 in thymocytes, recombination is not required for thymocytes to undergo p53-mediated apoptosis (12, 44). Moreover, although double-strand breaks are likely to occur in unirradiated epithelial cells of the small intestine due to errors in replication (5), such breaks would also be expected in the actively dividing cells of the colon, which do not show an elevated frequency of apoptosis. Normal levels of $p90^{MDM2}$ may nullify the effects of an unidentified signal intrinsic, for example, to epithelial cells in crypts of the small intestine but lacking in colonic epithelial cells. Alternatively, it may be that no signal is required to activate the apoptotic function of p53 other than one that inhibits $p90^{MDM2}$. If the second explanation is correct, this implies that tissue-specific differences in p53-mediated apoptosis are mediated through events downstream of p53, since only a subset of tissues underwent p53-mediated apoptosis when levels of $p90^{MDM2}$ were reduced, whereas all *mdm2*$^{puro/\Delta 7\text{-}12}$ tissues tested showed an increase in the transcriptional activation function of p53.

Regulation of *mdm2* expression. Our results demonstrate that *mdm2* is critical for homeostasis, yet little is known about the mechanisms that regulate expression of *mdm2* and the function of $p90^{MDM2}$ in tissues. The p53-MDM2 autoregulatory loop model proposes that p53 regulates its own activity by determining the level of its inhibitor, $p90^{MDM2}$ (1, 49, 60). However, our laboratory and others have shown that p53 does not regulate basal levels of *mdm2* expression in tissues (31, 37). In fact, 80 to 90% of *mdm2* mRNA in murine tissues is transcribed from an upstream promoter that is unresponsive to p53 (22, 37). The unidentified transcription factors that regulate this promoter may be critical for controlling p53, since the level of $p90^{MDM2}$ correlates with the level of *mdm2* mRNA transcribed from this promoter in murine testis, thymus, brain, and heart (7, 48). Although the level of $p90^{MDM2}$ varies considerably among wild-type tissues (48), here we show that it is sufficient to keep the transcriptional activation and apoptotic functions of p53 low or undetectable in all tissues tested. In addition to the level of $p90^{MDM2}$, posttranslational modifications that alter the activity of $p90^{MDM2}$ may be critical for determining the activity of p53.

Specific activity of p53 is elevated in *mdm2*$^{puro/\Delta 7\text{-}12}$ thymocytes. In *mdm2*$^{puro/\Delta 7\text{-}12}$ thymocytes, the percentage of apoptotic cells is increased approximately threefold in the absence of an apparent increase in the level of p53. The simplest interpretation of these data is a model in which the level of $p90^{MDM2}$ in *mdm2*$^{puro/\Delta 7\text{-}12}$ mice is sufficiently low to allow the transcriptional activation domain of p53 to interact more efficiently with the transcriptional machinery but high enough to ubiquitinate p53. The finding that p53 does not accumulate in the nuclei of *mdm2*$^{puro/\Delta 7\text{-}12}$ thymocytes is consistent with a normal level of ubiquitination of p53, since nuclear export of p53 is enhanced by ubiquitination. In fact, our observation that whole-body irradiation does not result in a greater accumulation of p53 in *mdm2*$^{puro/\Delta 7\text{-}12}$ thymocytes than in wild-type thymocytes suggests that the level of $p90^{MDM2}$ is not rate-limiting for controlling the level of p53 in this cell type. In the *mdm2*$^{puro/\Delta 7\text{-}12}$ spleen, the level of p53 was slightly elevated (less than twofold). However, p53 induced p21 expression 10-fold in this tissue, demonstrating that the specific activity of p53 is increased when *mdm2* expression is reduced. Conditional deletion of *mdm2* resulted in enhanced accumulation of p53 protein in the spleen, indicating that $p90^{MDM2}$ does regulate the level of p53 in this homeostatic tissue.

***mdm2* protects against the lethal effects of radiation.** The $p90^{MDM2}$/p53 interaction is a potential target for adjuvant chemotherapy (2). This work provides in vivo evidence for the feasibility of such approaches. The activity of p53 is exquisitely balanced, as evidenced by the increased radiosensitivity of *mdm2*$^{puro/+}$ mice, in which *mdm2* expression is decreased approximately 20%. Prior to the work presented here, there was no evidence that partial inhibition of $p90^{MDM2}$ would be sufficient to activate p53 in vivo. Moreover, the fact that a small decrease in $p90^{MDM2}$ activates p53 and sensitizes cells to radiation suggests that efficient inhibition of $p90^{MDM2}$ function would not be required in order for proposed adjuvant chemotherapies to be efficacious.

Our work has further implications for the design of adjuvant therapies to activate p53, as it suggests that the ubiquitin ligase function of $p90^{MDM2}$ may not be the optimal target for inhibition. Drugs that target this function of $p90^{MDM2}$ may need to be extremely efficient in order to increase the level of p53. However, targeting the physical interaction between $p90^{MDM2}$ and p53 would appear likely to increase the activity of p53 and synergize with primary cancer therapies. Finally, the fact that few tissues undergo p53-mediated apoptosis in response to decreases in *mdm2* implies that most nontumor tissues will be spared by adjuvant therapies that target the p53/$p90^{MDM2}$ interaction. Based on a recent report suggesting that elevated levels of p53 activity accelerate aging (56), one might speculate that drugs inhibiting $p90^{MDM2}$ would cause aging. However, no evidence for increased aging has been seen in *mdm2*$^{puro/\Delta 7\text{-}12}$ mice up to 22 months of age. Thus, combined with primary therapies targeted to tumor sites, adjuvant therapies that inhibit $p90^{MDM2}$ may in fact provide good tumor specificity.

ACKNOWLEDGMENTS

We acknowledge the expert assistance of the Transgenic Animal Facility and the Flow Cytometry Facility of the Comprehensive Cancer Center of the University of Wisconsin. We are grateful to A. Vaccaro and D. Monson for expert technical assistance and to D. Austin for generously providing statistical expertise. S. Jones (University of Massachusetts) provided mice heterozygous for the *mdm2*$^{\Delta 7\text{-}12}$ allele and *mdm2* genomic plasmids. We are grateful to A. Messing, J. Petrini, T. Prolla (University of Wisconsin), and A. Bradley (Sanger Centre,

Cambridge, United Kingdom) for help and advice in targeting embryonic stem cells. We thank A. Liem and P. Lambert for *p53*-null mice and E. Sandgren for *R26-Cre* mice. The expertise of pathologist H. Pitot is greatly appreciated.

This work was supported by funds from NIH grant CA-07175 to the McArdle Laboratory for Cancer Research, by NIH grant CA-14520 to the University of Wisconsin Comprehensive Cancer Center Flow Cytometry Facility, and by NIH grant CA-70718 to M.E.P. S.M.M. and J.M. were supported by NIH Predoctoral Training grants CA-09135 and GM-07215, respectively.

REFERENCES

1. **Barak, Y., T. Juven, R. Haffner, and M. Oren.** 1993. *mdm2* expression is induced by wild-type p53 activity. EMBO J. **12:**461–468.
2. **Böttger, A., V. Böttger, A. Sparks, W.-L. Liu, S. F. Howard, and D. P. Lane.** 1997. Design of a synthetic MDM2-binding mini protein that activates the p53 response *in vivo*. Curr. Biol. **7:**860–869.
3. **Bouvard, V., T. Zaitchouk, M. Vacher, A. Duthu, M. Canivet, C. Choisy-Rossi, M. Nieruchalski, and E. May.** 2000. Tissue- and cell-specific expression of the p53 target genes *bax*, *fas*, *mdm2* and *waf1/p21* before and following ionizing irradiation in mice. Oncogene **19:**649–660.
4. **Chen, L., S. Agrawal, W. Zhou, R. Zhang, and J. Chen.** 1998. Synergistic activation of p53 by inhibition of *mdm2* expression and DNA damage. Proc. Natl. Acad. Sci. USA **95:**195–200.
5. **Costanzo, V., K. Robertson, M. Bibikova, E. Kim, D. Grieco, M. Gottesman, D. Carroll, and J. Gutier.** 2001. Mre11 protein complex prevents double-strand break accumulation during chromosomal DNA replication. Mol. Cell **8:**137–147.
6. **Donehower, L. A., M. Harvey, B. L. Slagle, M. J. McArthur, C. A. Montgomery, Jr., J. S. Butel, and A. Bradley.** 1992. Mice deficient for p53 are developmentally normal but susceptible to spontaneous tumours. Nature **356:**215–221.
7. **Fakharzadeh, S. S., S. P. Trusko, and D. L. George.** 1991. Tumorigenic potential associated with enhanced expression of a gene that is amplified in a mouse tumor cell line. EMBO J. **10:**1565–1569.
8. **Freedman, D. A., and A. J. Levine.** 1998. Nuclear export is required for degradation of endogenous p53 by *mdm2* and human papillomavirus E6. Mol. Cell. Biol. **18:**7288–7293.
9. **Gavrieli, Y., Y. Sherman, and S. A. Ben-Sasson.** 1992. Identification of programmed cell death in situ via specific labeling of nuclear DNA fragmentation. J. Cell Biol. **119:**493–501.
10. **Gottlieb, E., R. Haffner, A. King, G. Asher, P. Gruss, P. Lonai, and M. Oren.** 1997. Transgenic mouse model for studying the transcriptional activity of the p53 protein: age- and tissue-dependent changes in radiation-induced activation during embryogenesis. EMBO J. **16:**1381–1390.
11. **Grippo, P. J., P. S. Nowlin, R. D. Cassaday, and E. Sandgren.** 2002. Cell-specific transgene expression from a widely transcribed promoter with Cre/Lox in mice. Genesis **32:**277–286.
12. **Guidos, C. J., C. J. Williams, I. Grandal, G. Knowles, M. T. F. Huang, and J. S. Danska.** 1996. V(D)J recombination activates a p53-dependent DNA damage checkpoint in *scid* lymphocyte precursors. Genes Dev. **10:**2038–2054.
13. **Harvey, M., A. T. Sands, R. S. Weiss, M. E. Hegi, R. W. Wiseman, P. Pantazis, B. C. Giovanella, M. A. Tainsky, A. Bradley, and L. A. Donehower.** 1993. *In vitro* growth characteristics of embryo fibroblasts isolated from p53-deficient mice. Oncogene **8:**2457–2467.
14. **Haupt, Y., S. Rowan, E. Shaulian, K. Vousden, and M. Oren.** 1995. Induction of apoptosis in HeLa cells by transactivation deficient p53. Genes Dev. **9:**2170–2183.
15. **Haupt, Y., R. Maya, A. Kazaz, and M. Oren.** 1997. MDM2 promotes the rapid degradation of p53. Nature **387:**296–299.
16. **Hinds, P. W., C. A. Finlay, A. B. Frey, and A. J. Levine.** 1987. Immunological evidence for the association of p53 with a heat shock protein, hsc70, in p53-plus-*ras*-transformed cell lines. Mol. Cell. Biol. **7:**2863–2869.
17. **Hollstein, M., M. Hergenhahn, Q. Yang, H. Bartsch, Z. Q. Wang, and P. Hainaut.** 1999. New approaches to understanding p53 gene mutation spectra. Mutat. Res. **431:**199–209.
18. **Honda, R., H. Tanaka, and H. Yasuda.** 1997. Oncoprotein MDM2 is a ubiquitin ligase E3 for tumor suppressor p53. FEBS Lett. **420:**25–27.
19. **Ikuta, K., N. Uchida, J. Friedman, and I. L. Weissman.** 1992. Lymphocyte development from stem cells. Annu. Rev. Immunol. **10:**739–783.
20. **Jacks, T., L. Remington, B. O. Williams, E. M. Schmitt, S. Halachmi, R. T. Bronson, and R. A. Weinberg.** 1994. Tumor spectrum analysis in *p53*-mutant mice. Curr. Biol. **4:**1–7.
21. **Jones, S. N., A. E. Roe, L. A. Donehower, and A. Bradley.** 1995. Rescue of embryonic lethality in MDM2-deficient mice by absence of p53. Nature **378:**206–208.
22. **Juven, T., Y. Barak, A. Zauberman, D. L. George, and M. Oren.** 1993. Wild-type p53 can mediate sequence-specific transactivation of an internal promoter within the *mdm2* gene. Oncogene **8:**3411–3416.
23. **Kastan, M. B., O. Onyekwere, D. Sidransky, B. Vogelstein, and R. W. Craig.** 1991. Participation of p53 protein in the cellular response to DNA damage. Cancer Res. **51:**6304–6311.
24. **Kastan, M. B., Q. Zhan, W. S. El-Deiry, F. Carrier, T. Jacks, W. V. Walsh, B. S. Plunkett, B. Vogelstein, and A. J. Fornace.** 1992. A mammalian cell cycle checkpoint pathway utilizing p53 and GADD45 is defective in ataxia-telangiectasia. Cell **71:**587–597.
25. **Komarova, E. A., M. V. Chernov, R. Franks, K. Wang, G. Armin, C. R. Zelnick, D. M. Chin, S. S. Bacus, G. R. Stark, and A. V. Gudkov.** 1997. Transgenic mice with p53-responsive *lacZ*: p53 activity varies dramatically during normal development and determines radiation and drug sensitivity *in vivo*. EMBO J. **16:**1391–1400.
26. **Komarova, E. A., K. Christov, A. I. Faerman, and A. V. Gudkov.** 2000. Different impact of p53 and p21 on the radiation response of mouse tissues. Oncogene **19:**3791–3798.
27. **Kubbutat, M. H. G., S. N. Jones, and K. H. Vousden.** 1997. Regulation of p53 stability by MDM2. Nature **387:**299–303.
28. **Kubbutat, M. H. G., R. L. Ludwig, A. J. Levine, and K. H. Vousden.** 1999. Analysis of the degradation function of MDM2. Cell Growth Differ. **10:**87–92.
29. **Kuhn, R., F. Schwenk, M. Aguet, and K. Rajewsky.** 1995. Inducible gene targeting in mice. Science **269:**1427–1429.
30. **Leach, F. S., T. Tokino, P. Meltzer, M. Burrell, J. D. Oliner, S. Smith, D. E. Hill, D. Sidransky, K. Kinzler, and B. Vogelstein.** 1993. p53 mutation and *mdm2* amplification in human soft tissue sarcomas. Cancer Res. **53:**2231–2234.
31. **Leveillard, T., P. Gorry, K. Niederreither, and B. Wasylyk.** 1998. *mdm2* expression during mouse embryogenesis and the requirement of p53. Mech. Dev. **74:**189–193.
32. **Lowe, S. W., H. E. Ruley, T. Jacks, and D. E. Housman.** 1993. p53-dependent apoptosis modulates the cytotoxicity of anticancer agents. Cell **74:**957–967.
33. **Lowe, S. W., S. Bodis, A. McClatchey, L. Remington, H. E. Ruley, D. E. Fisher, D. E. Housman, and T. Jacks.** 1994. p53 status and the efficacy of cancer therapy *in vivo*. Science **266:**807–810.
34. **MacCallum, D. E., T. R. Hupp, C. A. Midgley, D. Stuart, S. J. Campbell, A. Harper, F. S. Walsh, E. G. Wright, A. Balmain, D. P. Lane, and P. A. Hall.** 1996. The p53 response to ionizing radiation in adult and developing murine tissues. Oncogene **13:**2575–2587.
35. **Macleod, K. F., N. Sherry, G. Hannon, D. Beach, T. Tokino, K. Kinzler, B. Vogelstein, and T. Jacks.** 1995. p53-dependent and -independent expression of p21 during cell growth, differentiation and DNA damage. Genes Dev. **9:**935–944.
36. **McDonnell, T. J., R. Montes de Oca Luna, S. Cho, L. Amelse, A. Chavez-Reyes, and G. Lozano.** 1999. Loss of one but not two *mdm2* null alleles alters the tumor spectrum in p53 null mice. J. Pathol. **188:**322–328.
37. **Mendrysa, S. M., and M. E. Perry.** 2000. The p53 tumor suppressor protein does not regulate expression of its own inhibitor, MDM2, except under conditions of stress. Mol. Cell. Biol. **20:**3023–3030.
38. **Mendrysa, S. M., M. K. McElwee, and M. E. Perry.** 2001. Characterization of the 5′ and 3′ untranslated regions in murine *mdm2* mRNAs. Gene **264:**139–146.
39. **Merritt, A. J., C. S. Potten, C. J. Kemp, J. A. Hickman, A. Balmain, D. P. Lane, and P. A. Hall.** 1994. The role of *p53* in spontaneous and radiation-induced apoptosis in the gastrointestinal tract of normal and p53-deficient mice. Cancer Res. **54:**614–617.
40. **Midgley, C. A., B. Owens, C. V. Briscoe, D. B. Thomas, D. P. Lane, and P. A. Hall.** 1995. Coupling between gamma irradiation, p53 induction and the apoptotic response depends upon cell type *in vivo*. J. Cell Sci. **108:**1843–1848.
41. **Midgley, C. A., J. M. P. Desterro, M. K. Saville, S. Howard, A. Sparks, R. T. Hay, and D. P. Lane.** 2000. An N-terminal $p14^{ARF}$ peptide blocks MDM2-dependent ubiquitination *in vitro* and can activate p53 *in vivo*. Oncogene **19:**2312–2323.
42. **Momand, J., G. P. Zambetti, D. C. Olson, D. George, and A. J. Levine.** 1992. The *mdm-2* oncogene product forms a complex with the p53 protein and inhibits p53-mediated transactivation. Cell **69:**1237–1245.
43. **Montes de Oca Luna, R., D. S. Wagner, and G. Lozano.** 1995. Rescue of early embryonic lethality in *mdm2*-deficient mice by deletion of *p53*. Nature **378:**203–206.
44. **Nacht, M., and T. Jacks.** 1996. V(D)J recombination is not required for the development of lymphoma in p53-deficient mice. Cell Growth Differ. **9:**131–138.
45. **Oliner, J. D., K. W. Kinzler, P. S. Meltzer, D. L. George, and B. Vogelstein.** 1992. Amplification of a gene encoding a p53-associated protein in human sarcomas. Nature **358:**80–83.
46. **Oliner, J. D., J. A. Pietenpol, S. Thiagalingam, J. Gyuris, K. W. Kinzler, and B. Vogelstein.** 1993. Oncoprotein MDM2 conceals the activation domain of tumor suppressor p53. Nature **362:**857–860.
47. **Parker, S. B., G. Eichele, P. Zhang, A. Rawls, A. T. Sands, A. Bradley, E. N. Olson, J. W. Harper, and S. J. Elledge.** 1995. p53-independent expression of $p21^{Cip1}$ in muscle and other terminally differentiating cells. Science **267:**1024–1027.
48. **Perry, M. E., S. M. Mendrysa, L. J. Saucedo, P. Tannous, and M. Holubar.**

2000. $p76^{MDM2}$ inhibits the ability of $p90^{MDM2}$ to destabilize p53. J. Biol. Chem. **275:**5733–5738.
49. **Prives, C.** 1998. Signaling to p53: breaking the MDM2-p53 circuit. Cell **95:**5–8.
50. **Roth, J. M., M. Dobbelstein, D. A. Freedman, T. Shenk, and A. J. Levine.** 1998. Nucleo-cytoplasmic shuttling of the hdm2 oncoprotein regulates the levels of the p53 protein via a pathway used by the human immunodeficiency virus rev protein. EMBO J. **17:**554–564.
51. **Sauer, B., and N. Henderson.** 1988. Site-specific DNA recombination in mammalian cells by the Cre recombinase of bacteriophage P1. Proc. Natl. Acad. Sci. USA **85:**5166–5170.
52. **Schutte, B., M. M. Reynders, C. L. van Assche, P. S. Hupperets, F. T. Bosman, and G. H. Blijham.** 1987. An improved method for the immunocytochemical detection of bromodeoxyuridine labeled nuclei with flow cytometry. Cytometry **8:**372–376.
53. **Shinkai, Y., G. Rathbun, K.-P. Lam, E. M. Oltz, V. Stewart, M. Mendelsohn, J. Charron, M. Datta, F. Young, A. M. Stall, and F. W. Alt.** 1992. RAG-2-deficient mice lack mature lymphocytes owing to inability to initiate V(D)J rearrangement. Cell **68:**855–867.
54. **Thut, C. J., J. A. Goodrich, and R. Tjian.** 1997. Repression of p53-mediated transcription by MDM2: a dual mechanism. Genes Dev. **11:**1974–1986.
55. **Todaro, G. J., and H. Green.** 1963. Qualitative studies of the growth of mouse embryo cells in culture and their development into established cell lines. J. Cell Biol. **17:**299–313.
56. **Tyner, S. D., S. Venkatachalam, J. Choi, S. Jones, N. Ghebranious, H. Igelmann, X. Lu, G. Soron, B. Cooper, C. Brayton, S. H. Park, T. Thompson, G. Karsenty, A. Bradley, and L. A. Donehower.** 2002. p53 mutant mice that display early ageing-associated phenotypes. Nature **415:**45–53.
57. **Vogelstein, B., D. Lane, and A. J. Levine.** 2000. Surfing the p53 network. Nature **408:**307–310.
58. **Westphal, C. H., K. P. Hoyes, C. E. Canman, X. Huang, M. B. Kastan, J. H. Hendry, and P. Leder.** 1998. Loss of atm radiosensitizes multiple p53 null tissues. Cancer Res. **58:**5637–5639.
59. **Willerford, D. M., W. Swat, and F. W. Alt.** 1996. Developmental regulation of V(D)J recombination and lymphocyte differentiation. Curr. Opin. Genet. Dev. **6:**603–609.
60. **Wu, X., J. H. Bayle, D. Olson, and A. J. Levine.** 1993. The p53-*mdm-2* autoregulatory feedback loop. Genes Dev. **7:**1126–1132.
61. **Yonish-Rouach, E., D. Resnitzky, J. Lotem, L. Sachs, A. Kimchi, and M. Oren.** 1991. Wild-type p53 induces apoptosis of myeloid leukemic cells that is inhibited by interleukin-6. Nature **352:**345–347.